

History-Dependence and Ageing in a Periodic Long-Range Josephson Array

P. Chandra,¹ M.V. Feigelman,² L.B. Ioffe^{2,3} and D.M. Kagan²

¹*NEC Research Institute, 4 Independence Way, Princeton NJ 08540*

²*Landau Institute for Theoretical Physics, Moscow, RUSSIA*

³*Department of Physics, Rutgers University, Piscataway, NJ 08855*

History-dependence and ageing are studied in the low-temperature glass phase of a long-range periodic Josephson array. This model is characterized by two parameters, the number of wires ($2N$) and the flux per unit strip (α); in the limit $N \rightarrow \infty$ and fixed $\alpha \ll 1$ the dynamics of the model are described by the set of coupled integral equations, which coincide with those for the $p = 4$ *disordered* spherical model. Below the glass transition we have solved these equations numerically in a number of different regimes.

We observe power-law ageing after a fast quench with an exponent that decreases rapidly with temperature. After slow cooling to a not-too-low temperature, we see ageing characterized by the appearance of a new time scale which has a power law dependence on the cooling rate. By contrast if the array is cooled slowly to very low temperatures the ageing disappears. The physical consequences of these results in different cooling regimes are discussed for future experiment.

We also study the structure of the phase space in the low temperature glassy regime. Analytically we expect an exponential number of metastable states just below the glass transition temperature with vanishing mutual overlap, and numerical results indicate that this scenario remains valid down to zero temperature. Thus in this array there is no further subdivision of metastable states. We also investigate the probability to evolve to different states given a starting overlap, and our results suggest a broad distribution of barriers.

I. INTRODUCTION

The essential features underlying the physics of glass formation remain elusive. A glassy system has a “memory” of its past history; it breaks ergodicity without thermodynamic selection of a unique state thereby defying description by the standard Gibbs methods. Though glass formation in the absence of disorder is a widespread phenomenon, it remains poorly understood even at the mean-field level. Several infinite-range models for disorder-free glassiness have been proposed;¹ the majority were studied via a mapping to intrinsically random systems.² This approach relies on the observation that certain infinite-range periodic and random models have identical leading order (in $1/N$) high-temperature expansions. This correspondance is assumed to persist at low temperatures. Crystalline phase(s), which could appear in a periodic model, are missed by such a treatment; however the usual working assumption is that they are dynamically inaccessible. Recently a glass transition in a periodic, long-range Josephson array has been identified and characterized^{3,4} using a generalized Thouless-Anderson-Palmer (TAP) approach.⁵ This model can be studied directly (without a mapping to a disordered system) because it has *two* expansion parameters: the first is the usual $1/N$ inherent to a long-range model; the second is α , the flux per unit strip, where the condition $\alpha \ll 1$ further restricts the number of contributing diagrams to be a small subset of all those appearing to $O(\frac{1}{N})$. The existence of α as an expansion parameter suggests that the crystalline phase(s) are inaccessible (or do not exist) for small values of α . We note that for $\alpha = 1$ there exist non-trivial ground-states for an array with prime N which are certainly missed by perturbative methods. In this particular case, any sequence of complex numbers (representing the order parameters associated with each wire) of unit magnitude whose discrete Fourier transform has a flat spectrum yields a ground-state.⁶ This mathematical problem has been studied extensively in the context of number theory, beginning with the work of Gauss.⁷

Another key feature of the periodic Josephson array is that it can be constructed in the laboratory; the physical requirements imposed by the theory on its realization have been discussed elsewhere.⁸ Measurement of the a.c. response to a small time-varying field in the fabricated array should probe its diverging relaxation time at the glass transition.^{4,8} In this paper we study the behavior of this periodic network in its low-temperature non-ergodic regime. We find both history-dependence and ageing, and the physical consequences of these results for different cooling regimes are discussed for future experiment.

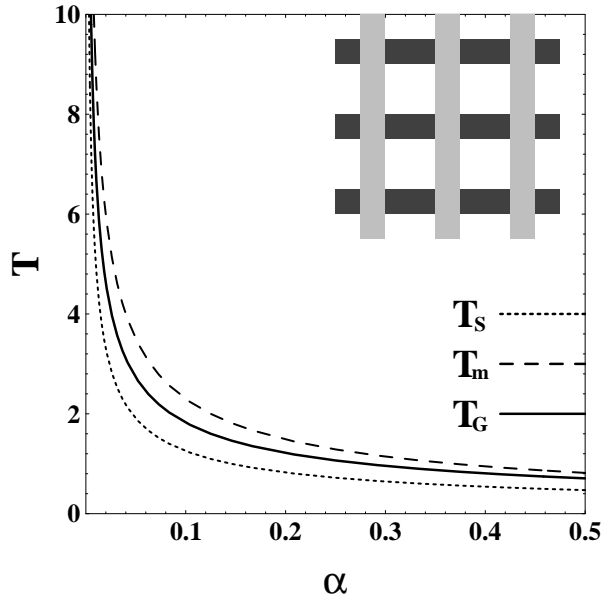


Fig 1. The phase diagram of the array (inset). Here T_G , T_m and T_S are the temperatures associated with the dynamical instability, “superheating”, and a speculated equilibrium transition as discussed in the text.

The system of our study is a stack of two mutually perpendicular sets of N parallel thin superconducting wires with Josephson junctions at each node (Figure 1) that is placed in an external transverse field H . The classical thermodynamic variables of this array are the $2N$ superconducting phases associated with each wire. In the absence of an external field the phase differences would be zero at each junction, but this is not possible for finite H and the phases are thus frustrated. Here we assume that the Josephson couplings are sufficiently small so that the induced fields are negligible in comparison with H , an important point for the experimental realization of this network.⁸ We can therefore describe the array by the Hamiltonian

$$\mathcal{H} = - \sum_{m,n}^{2N} s_m^* \mathcal{J}_{mn} s_n \quad (1)$$

where \mathcal{J}_{mn} is the coupling matrix

$$\hat{\mathcal{J}} = \begin{pmatrix} 0 & \hat{J} \\ \hat{J}^\dagger & 0 \end{pmatrix} \quad (2)$$

with $J_{jk} = \frac{J_0}{\sqrt{N}} \exp(2\pi i \alpha j k / N)$ and $1 \leq (j, k) \leq N$ where $j(k)$ is the index of the horizontal (vertical) wires; $s_m = e^{i\phi_m}$ where the ϕ_m are the superconducting phases of the $2N$ wires. Here we have introduced the flux per unit strip, $\alpha = NHl^2/\Phi_0$, where l is the inter-node spacing and Φ_0 is the flux quantum; the normalization has been chosen so that T_G does not scale with N .

Because every horizontal (vertical) wire is linked to every vertical (horizontal) wire, the connectivity in this model is high (N) and it is accessible to a mean-field treatment.⁹ For $\frac{1}{N} \ll \alpha < 1$ there exist an extensive number of metastable solutions separated by barriers that scale³ with N . A similar long-range network with disorder was previously found to display a spin glass transition⁹ for $\alpha \gg \frac{1}{N}$; in the absence of short-range phase coherence between wires ($\alpha \gg 1$), it was mapped onto the Sherrington-Kirkpatrick model.¹⁰ Physically this glassy behavior occurs because the phase

differences associated with the couplings, J_{jk} , acquire random values and fill the interval $(0, 2\pi)$ uniformly. For the periodic case, this condition is satisfied in the “incommensurate window” $\frac{1}{N} \ll \alpha \leq 1$; here the magnetic unit cell is larger than the system size so that the simple “crystalline” phase is inaccessible.³ There are thus no special field values where the number of low-temperature solutions are not extensive, in contrast to the situation for $\alpha > 1$. Of course, we cannot exclude the possibility that at low temperatures a single low-lying state appears; however it seems very likely that even in this case it will be irrelevant because the system is trapped in one of the many metastable glassy states. Furthermore we have not observed such states in our direct numerical simulations of $\alpha = 1$ array.

In the thermodynamic limit of $N \rightarrow \infty$ (with fixed area), the system is accessible to a static and dynamical high-temperature study;^{3,4} this was performed using a modified TAP method.⁵ This will be discussed in more detail when the coupled dynamical equations are derived in Section II; at temperatures above the dynamic instability the system is still in equilibrium and these equations can be solved analytically. The glass transition is characterized by a diverging relaxation time and a jump in the Edwards-Anderson order parameter, and does *not* coincide with an accompanying static transition. This calculated glass transition temperature (T_G) assumes that cooling from high temperatures occurs infinitesimally slowly; in practice, the system’s effective glass transition temperature ($T_G^{eff} > T_G$) will correspond to the system’s failure to equilibrate and will be a function of its finite cooling time-scale. For the sake of notational simplicity, we will not distinguish between the effective and the “adiabatic” glass transition temperature in the text that follows unless explicitly stated.

Below the glass transition temperature (T_G), the system can no longer equilibrate. In contrast to the situation for $T > T_G$, the response and the correlation functions are *not* a function of time differences but rather are history-dependent; furthermore we can no longer relate them with the fluctuation-dissipation theorem. This makes the solution of these equations rather complicated. The low-temperature state of the system is determined by the sample history; here we shall consider the simplest scenario in which the temperature is reduced linearly from an initial T_i slightly above T_G to a final temperature $T_f (< T_G)$ in a time t_c . The final state of the system at time $t > t_c$ is controlled by both time-scales t and t_c , and we expect qualitatively different behavior depending on their relative magnitude. Here we shall focus on the limiting cases $t \gg t_c$ and $t = t_c$.

Physically in the limit of very fast cooling ($t \gg t_c$), we expect the state immediately following the quench to have minimal overlap with that observed at time t so that $D_{tt'} \rightarrow 0$. Assuming that the solutions of the dynamical equations are well-defined in the limit when the microscopic time-scale goes to zero, we have only two time-scales in the problem: t and t' . In this case $D_{tt'}$ may depend only on their ratio t'/t on dimensional grounds: $D_{tt'} = d(\frac{t'}{t})$. Since $d(0) = 0$ we expect $\lim_{t'/t \rightarrow 0} d(\frac{t'}{t}) = (\frac{t'}{t})^\gamma D_0$, and this functional form of $D_{tt'}$ remains^{11,12} at larger values of $(\frac{t'}{t})$. Similarly in this fast-cooling regime we expect $\lim_{t'/t \rightarrow 0} G_{tt'} = \frac{1}{t'} (\frac{t'}{t})^\gamma G_0$, so that in the limit of small (t'/t) there is a quasi-FDT relation ($G \propto D'$), which remains valid^{11,12} over the full range $0 < (t'/t) < 1$.

The other limiting case is that of slow cooling ($t = t_c$), where we expect that the correlation and response functions will have their only time-dependence through the specified cooling process $\tau(t)$ where $\tau \equiv (\frac{T_G - T}{T_G})$: $D_{tt'} = d[\tau(t), \tau(t')]$ and $G_{tt'} = \frac{d\tau(t')}{dt'} g[\tau(t), \tau(t')]$. If this conjecture is correct, it implies that the system has a non-decaying memory of its past history. Of course this assumes again that the solutions to the dynamical equations are well-defined in the limit of vanishing microscopic time-scales. For the Sherrington-Kirkpatrick model,¹⁰ this “adiabatic ansatz” for linear $\tau(t)$ leads¹³ to the solutions $d(t, t') = \tau_{t'}$ and $g(t, t') = 2\tau_{t'}$, which result in a field-cooled susceptibility in qualitative agreement with a previous equilibrium result.¹⁴ However application of the same method to the $p = 4$ Ising model leads to a delta-function solution for the response function;¹⁵ this form is worrisome given the original adiabatic nature of the ansatz. However, in principle the response could be broadened to be long compared to the microscopic time-scale but short compared to the final measurement time.¹⁵ When we started our numerical study of this problem, our expectations were therefore that the only time scale in the slow cooling process is set by the cooling rate, $t^* \equiv (\frac{dT}{dt})^{-1}$, and that the response and the correlation functions depend only on the ratios t/t^* and t'/t^* as indicated in the $t = t_c$ column of Table 1. This hypothesis turned out to be only partially correct. Instead we have found that indeed just below T_G the correlation and response functions depend only on the ratios t/t^* and t'/t^* but t^* is a *new* time-scale $t^* \equiv (\frac{dt}{d\tau})^{1-\eta(T)}$ that emerges in this cooling regime; however there is evidence that the exponent η vanishes at low temperatures, indicating that “adiabatic cooling” is recovered. We note that a finite value of η implies a decaying memory and hence ageing, and thus the disappearance of η means that the system recovers its memory and thus “rejuvenates” at low temperatures.

Our expectations for the three cooling regimes are summarized in Table I. In Section II. we derive the dynamical equations for the array in the low-field ($\alpha \ll 1$) regime. The system goes out of equilibrium at a temperature T_G (determined by the cooling rate), and we study its low-temperature ($T < T_G$) behavior numerically in all three cooling regimes; our results are presented in Section III.

We also probe the structure of phase space in this glassy regime (Section IIID) where the periodic array is stuck in one

of an extensive number of metastable states.³ What happens to these states when the temperature is decreased? Each state, formed at T_G , may evolve smoothly; alternatively it can further subdivide as in the case of the (disordered) Sherrington-Kirkpatrick model. We find that in this periodic array there is no further subdivision down to zero temperatures, and that the number of metastable states remains exponentially large. We also learn that though these states are equidistant in phase space, their associated basins of attraction are rather complicated. We conclude with a discussion of the physical consequences for experiment (Section IV), a brief summary and with projects for future work.

TABLE I. Three distinct regimes and their associated response ($D_{tt'}$ and correlation ($G_{tt'}$) functions when the system is quenched out-of-equilibrium ($t < t_R$); here t , t_r and t_c are the measurement, relaxation and cooling times respectively, and t^* is a time-scale which is a function of the cooling rate ($\frac{dT}{dt}$).

$t \gg t_c$	$t \gtrsim t_c$	$t = t_c$
$D_{tt'} = \left(\frac{t'}{t}\right)^\gamma D_0$???	$D_{tt'} = d\left(\frac{t'}{t^*}, \frac{t}{t^*}\right)$
$G_{tt'} = xD'_{tt'}$???	$G_{tt'} = \frac{1}{t^*}g\left(\frac{t'}{t^*}, \frac{t}{t^*}\right)$
		$t^* = f\left(\frac{dT}{d\tau}\right)$

II. THE DYNAMICAL EQUATIONS

The time-dependent properties of a glass are particularly distinctive, and thus we begin our study with a discussion of the self-consistent equations describing the dynamics of the periodic Josephson array. For the sake of convenience, we shall refer to the network model described by the Hamiltonian (1) in “magnetic” language so that each “spin” $s_m = e^{i\phi_m}$ is associated with the phase of a superconducting wire labelled by “site index” m . We presume that the system’s long-time behavior can be described by that of soft spins with pure relaxational modes, since intrinsic single-spin dynamics should be irrelevant on these time-scales. More specifically we introduce a “constraining potential” $V(s_i) = V_0(|s|^2 - 1)^2$ at each site that restricts the magnitude of each spin, $|s_i| \approx 1$, and then assume the equations of motion

$$\tau_b \dot{s}_i = -\frac{1}{T} \frac{\partial(\mathcal{H} + V)}{\partial s_i^*} + \zeta_i \quad (3)$$

where τ_b is a microscopic time-scale; the effects of a coupled heat bath are represented by a time-varying Gaussian random field $\zeta_i(t)$ with zero mean and variance

$$\langle \zeta_i(t) \zeta_j(t') \rangle = 2\tau_b \delta_{ij} \delta(t - t') \quad (4)$$

where the brackets refer to an average over the noise. This Langevin equation (3) reproduces the dynamics of the overdamped Josephson array⁸ with effective resistance R if $\tau_b = \frac{R_Q \hbar}{R T}$ and $V_0 \rightarrow \infty$ where $R_Q = \frac{\hbar}{4e^2}$; here $R = \frac{R_0}{N}$ where R_0 is the individual junction resistance since the circuit elements in the long-range array operate in parallel.⁸

The physical quantities of interest here are the dynamical cumulants of the “spin” variables averaged over the noise. In particular, we would like to determine the time-dependant two-spin correlation function

$$D_{mn}(t, t') = \langle s_m(t) s_n^*(t') \rangle \quad (5)$$

and the linear response

$$G_{mn}(t, t') = \frac{\partial \langle s_m(t) \rangle}{\partial h_n(t')}, \quad t > t' \quad (6)$$

where again the angular brackets refer to an average over $\zeta_i(t)$. We note that $G_{mn}(t, t')$ is a susceptibility with respect to a “theorist’s” field h_n conjugate to a spin $s_n = e^{i\phi_n}$, and thus cannot be measured directly; however once known, $G_{mn}(t, t')$ can be used to determine the ac-response to a time-varying physical external field $H(t)$ which is experimentally accessible.⁴

Exploiting the fact that the Langevin noise $\zeta_i(t)$ is Gaussian and uncorrelated in space and time, we can perform the noise averages in (5) and (6) using a functional integral formulation;^{16,17} details of this technique can be found elsewhere.¹⁸ For example, the two-spin dynamical correlation function is given by the expression

$$D_{mn}(t, t') = \langle s_m(t) s_n^*(t') \rangle = \int s_m(t) s_n^*(t) \exp \mathcal{A}[s, \hat{s}] \mathcal{D}s \mathcal{D}\hat{s}. \quad (7)$$

with the action

$$\mathcal{A}[s, \hat{s}] = \int dt \left[\hat{s} \left(\tau_b \dot{s} + \frac{1}{T} \frac{\partial(\mathcal{H} + V)}{\partial s^*} \right) + \tau_b \hat{s}^2 + h.c. \right] \quad (8)$$

where we have neglected the term arising from the functional Jacobian since it does not affect the system’s long-time behavior provided that causality is maintained; the latter is ensured by the diagrammatic treatment described below. The auxiliary field \hat{s} in a correlation function¹⁹ acts like a response term $\frac{\partial}{\partial h(t)}$ so that $G_{mn}(t, t') = \langle s_m(t) \hat{s}_n(t') \rangle$ can be determined by an expression analogous to (7).

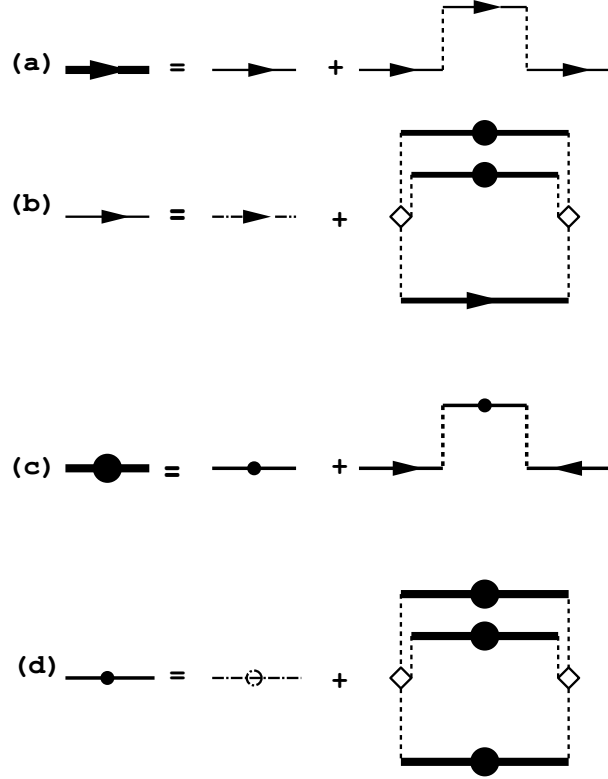


Fig 2. The diagrammatic expansion (to leading order in $1/N$) for the (a) response and the (b) correlation functions. Here the coupling matrix \mathcal{J} is represented by dashed lines, Γ is the single-site four-spin vertex shown as a diamond, \tilde{G}_ω (\tilde{D}_ω) is the single-site irreducible response (correlation) function, \mathbf{G} (\mathbf{D}) is the full response (correlation) function, and \tilde{G}_b (\tilde{D}_b) is the single-site bare response (correlation) function. The leading self-energy contributions to \tilde{G}_ω and \tilde{D}_ω (in $\alpha \ll 1$) are displayed in (c) and (d) respectively.

More specifically, we calculate the time-dependent correlation and response functions, $D_{mn}(t, t')$ and $G_{mn}(t, t')$ respectively, by resumming the terms in the $\frac{\hbar}{T}$ expansion of the generating functional associated with (8) which are leading order in $\frac{1}{N}$; this is a dynamical generalization^{3,8} of the Thouless-Anderson-Palmer approach⁵ where feedback through single-site Onsager terms play a crucial role. It is convenient to determine these response and correlation functions initially in the frequency-domain. The leading diagrams (in $\frac{1}{N}$) for \tilde{G}_ω are shown in Figure 2a; in the thermodynamic limit ($\lim N \rightarrow \infty$ with fixed array area) the subleading corrections to the response can be safely neglected.⁸ Summing the geometric series shown in Figure 2a, we obtain

$$\mathbf{G}_\omega = \frac{1}{\tilde{\mathbf{G}}_\omega^{-1} - \beta^2(\mathbf{J}\mathbf{J}^\dagger)\tilde{\mathbf{G}}_\omega} \quad (9)$$

for the response function connecting wires of the same type (horizontal/vertical); here we consider the local Green's functions \tilde{G}_ω that is irreducible with respect to the J_{ij} lines. The matrix $(J\mathbf{J}^\dagger)_{ij}$ depends only on the "distance" $i - j$ and acquires a simple form in Fourier space $(J\mathbf{J}^\dagger)_p = (J_0^2/\alpha)\theta(\alpha\pi - |p|)$; therefore in this representation the low-frequency contribution to the response function⁴ is

$$G^{(0)} = \int \frac{dp}{(2\pi)} \frac{\theta(\alpha\pi - |p|)}{\tilde{G}_\omega^{-1} - \frac{(\beta J_0)^2}{\alpha} \tilde{G}_\omega} + \frac{\theta(|p| - \alpha\pi)}{\tilde{G}_\omega^{-1}} \quad (10)$$

which is of primary interest in this problem. We note that the static limit ($\omega = 0$) of $T\tilde{G}_\omega^{-1}$ coincides with the locator, $A(T)$, discussed in previous work on this array;³ in the absence of feedback terms $\tilde{G}_0^{-1} = 1$. We also see in (10) that there is a static instability at $\tilde{G}_0^{-1} = G_c = \frac{\beta J_0}{\sqrt{\alpha}}$ in the vicinity of $T_0 = \frac{J_0}{\sqrt{\alpha}}$. For $\Theta = \frac{(T-T_0)}{T_0} \gg \sqrt{\alpha}$ all feedback terms are negligible and $\tilde{G}_\omega^{-1} \equiv \tilde{G}_b^{-1}(\omega) = \beta A(T) - i\omega\tau_b$ where τ_b is a microscopic time-scale. However at lower temperatures, $\Theta \leq \sqrt{\alpha}$, feedback effects introduce an additional frequency-dependent part of the local response

$$\tilde{G}_\omega = \tilde{G}_b(\omega) + \Sigma_\omega \quad (11)$$

as a self-energy (Σ_ω such that $\Sigma_0 = 0$) since we have chosen our normalization so that $\tilde{G}_0^{-1} = \beta A(T)$. The leading contribution in α to the self-energy Σ_ω is displayed in Figure 2b. We note that the self-energy contains a term $\hat{\mathbf{G}} = \beta_0 \mathbf{J}^\dagger \mathbf{G} \mathbf{J}$ where \mathbf{G} is the *full* response function and $\beta_0 = \frac{1}{T_0}$, and it is therefore convenient to write an equation for $\hat{\mathbf{G}}$. We shall use the identity

$$\mathbf{G} = (\mathbf{G} - \beta_0^2 \mathbf{J}^\dagger \mathbf{G} \mathbf{J}) + \hat{\mathbf{G}}, \quad \hat{\mathbf{G}} = \beta_0^2 \mathbf{J}^\dagger \mathbf{G} \mathbf{J} \quad (12)$$

and note that, since the matrix $\mathbf{J} \mathbf{J}^\dagger$ has only two eigenvalues, 0 and T_0^2 , the expression $(\mathbf{G} - \beta_0^2 \mathbf{J}^\dagger \mathbf{G} \mathbf{J}) = (\mathbf{1} - \beta_0^2 \mathbf{J}^\dagger \mathbf{J}) \mathbf{G} = (\mathbf{1} - \beta_0^2 \mathbf{J}^\dagger \mathbf{J}) \tilde{\mathbf{G}}$ projects only the zero eigenvalue contribution of $\mathbf{J} \mathbf{J}^\dagger$ in the denominator of (9). We note that $\tilde{\mathbf{G}}$ is diagonal so that the order of matrix multiplication is not important. $\hat{\mathbf{G}}$ is equivalent to the long-time part of the response function and is proportional to α (cf. (10)). Higher order terms in the self-energy will thus contain higher powers of α , and thus we conjecture that for $\alpha \ll 1$ these terms can be neglected; this will be justified later by the structure of the resulting solutions for \mathbf{G} and \mathbf{D} .

The retardation of the self-energy terms (cf. Fig. 2b and 2d) significantly affect the long-term behavior of the system. This feedback results in a diverging relaxation time and a dynamical instability⁴ at a temperature $T_G = (1 + \Theta_G) T_0$ where $\Theta_G = -\frac{3^{3/4}}{2^{1/2}} \alpha^{1/4}$.

For temperatures $T > T_G$ the response and correlation functions depend *only* on the time-differences, and thus can be related by the Fluctuation-Dissipation Theorem. However for $T < T_G$ this relation no longer holds and we must determine the correlation function independently. Analogous to our treatment above, we introduce $\tilde{\mathbf{D}}$ and $\hat{\mathbf{D}}$ as in equation (12):

$$\mathbf{D} = (\mathbf{D} - \beta_0^2 \mathbf{J}^\dagger \mathbf{D} \mathbf{J}) + \hat{\mathbf{D}}, \quad \hat{\mathbf{D}} = \beta_0^2 \mathbf{J}^\dagger \mathbf{D} \mathbf{J}. \quad (13)$$

where again we use $(\mathbf{D} - \beta_0^2 \mathbf{J}^\dagger \mathbf{D} \mathbf{J}) = (\mathbf{1} - \beta_0^2 \mathbf{J}^\dagger \mathbf{J}) \tilde{\mathbf{D}}$. The leading diagrams (in $\frac{1}{N}$) for \hat{D}_ω are shown in Figure 2c; the low-frequency contribution to this correlation function is

$$\hat{D}^{(0)} = \int \frac{dp}{(2\pi)} \frac{\theta(\alpha\pi - |p|)}{\tilde{G}_\omega^{-1} - \frac{(\beta J_0)^2}{\alpha} \tilde{G}_\omega} \hat{\Pi}_\omega \frac{1}{\tilde{G}_\omega^{-1} - \frac{(\beta J_0)^2}{\alpha} \tilde{G}_\omega} \quad (14)$$

where Π is an on-site self-energy contribution to \tilde{D}_ω . For long times and ($\frac{1}{N} <$) $\alpha \ll 1$

$$\hat{G}_{t_1, t_2} = \frac{\alpha}{a + 2 \frac{\partial}{\partial t_1} \tau_b - 2 \Sigma_{t_1, t_2}} \quad (15)$$

and

$$\hat{D}_{t_1, t_2} = \frac{\alpha}{a + 2 \frac{\partial}{\partial t_1} \tau_b - 2 \Sigma_{t_1, t_2}} \Pi_{t_1, t_2} \frac{1}{a + 2 \frac{\partial}{\partial t_1} \tau_b - 2 \Sigma_{t_1, t_2}} \quad (16)$$

where $a \equiv \beta(A - \frac{J_0^2}{\alpha A}) \approx 2\Theta$ for $\Theta \gg \sqrt{\alpha}$ and $a \approx -\frac{\alpha}{\Theta}$ for $-\Theta \gg \sqrt{\alpha}$ and A is the locator.⁴ Possible on-site self-energy terms, Σ and Π , displayed to leading order in α in Figures 2b and 2d, simplify in the limit of $\alpha \ll 1$. In this regime, which we consider here, we note from (15) and (16) that the slowly decaying parts of \hat{G} and \hat{D} scale with α . Therefore the dominant self-energy contributions contain the minimal number of these functions (cf. Figs. 2c and 2d respectively). We can therefore consider only the leading order feedback terms

$$\Sigma_{t_1, t_2} = \frac{3}{2} \hat{D}_{t_1, t_2}^2 \hat{G}_{t_1, t_2} \quad (17)$$

and

$$\Pi_{t_1, t_2} = \hat{D}_{t_1, t_2}^3 + 2\tau_b \delta_{t_1, t_2} \quad (18)$$

where \hat{G} and \hat{D} are as in (15) and (16) respectively, and we have approximated the four-spin vertex by its static value $\Gamma = -1$.

We now have expressions for the correlation and the response functions

$$\left(a_{t_1} + 2\tau_b \frac{\partial}{\partial t_1} - 2\Sigma_{t_1, t_2}\right) \hat{G}_{t_1, t_2} = \alpha \delta(t_1 - t_2) \quad (19)$$

$$\left(a_{t_1} + 2\tau_b \frac{\partial}{\partial t_1} - 2\Sigma_{t_1, t_2}\right) \hat{D}_{t_1, t_2} = \int \hat{D}_{t_1, t_2}^3 \hat{G}_{t_2, t'} dt' + 2\tau_b \hat{G}_{t_1, t_2}. \quad (20)$$

In order to solve these equations we also require a boundary condition for $\hat{D}(t, t)$, which follows from the definition (13) and the condition that $D_{i,i}(t, t) = 1$ so that

$$(1 - \alpha)\tilde{D}(t, t) + \hat{D}(t, t) = 1. \quad (21)$$

We only need to consider equation (21) to order $O(\alpha^{1/4})$ which allows us to neglect self-energy corrections to \tilde{D} (cf. Figure 2d) that scale as $\alpha^{3/4}$ in this case $\tilde{D}(t, t) \approx \tilde{D}^{(0)}(t, t)$ then $\hat{D}(t, t) \approx 1 - D^{(0)}(t, t)$. In the vicinity of the glass transition studied here, $-\Theta \sim \alpha^{1/4} \gg \sqrt{\alpha}$, we have⁴ $\tilde{D}_{tt}^{(0)} = \tilde{G}_{\omega=0}^{(0)} \approx (1 + \Theta)$ and therefore

$$\hat{D}_{t,t} = -\Theta_t. \quad (22)$$

This boundary condition and equations (19) and (20) form a closed system of equations.

We can simplify (19) and (20) by defining the parameters

$$t_0 = 2\tau_b \alpha^{-3/4} \quad \theta = -\Theta \alpha^{-1/4} \quad a_{t_1} = \tilde{a}_{t_1} \alpha^{3/4} \Theta_{t_1} \quad (23)$$

and the rescaled functions

$$\hat{D}_{t_1, t_2} = \alpha^{1/4} \theta_{t_1} d\left(\frac{t_1}{t_0 \theta_t}, \frac{t_2}{t_0 \theta_{t_2}}\right) \quad (24)$$

$$\hat{G}_{t_1, t_2} = \alpha^{1/4} \frac{1}{t_0} g\left(\frac{t_1}{t_0 \theta_t}, \frac{t_2}{t_0 \theta_{t_2}}\right) \quad (25)$$

to obtain the equations

$$\left(\tilde{a}_{t_1} + \frac{\partial}{\partial t_1}\right) g(t_1, t_2) - 3\theta_{t_1}^3 \int_{t_1}^{t_2} d^2(t_1, t') g(t_1, t') g(t', t_2) \theta_{t'} dt' = \delta(t_1 - t_2) \quad (26)$$

$$\begin{aligned} \left(\tilde{a}_{t_1} + \frac{\partial}{\partial t_1}\right) d(t_1, t_2) - 3\theta_{t_1}^2 \int_0^{t_1} d^2(t_1, t') g(t_1, t') g(t', t_2) \theta_{t'}^2 dt' \\ - \theta_{t_1}^3 \int_0^{t_2} d^3(t_1, t') g(t_2, t') \Theta_{t'} dt' - 2g(t_1, t_2) = 0 \end{aligned} \quad (27)$$

where we have used the leading order (in $\alpha \ll 1$) self-energy terms, (17) and (18). The boundary conditions, $d(t, t) = 1$ and

$$g(t_1, t_2)|_{t_1 \rightarrow t_2^+} = 1 \quad \frac{\partial}{\partial t_1} d(t_1, t_2) \Big|_{t_1 \rightarrow t_2^-} = 1 \quad (28)$$

yields another relation

$$\tilde{a}_t = 1 + 4\theta_t^3 \int_0^t d^3(t, t') g(t, t') \theta_t' dt' \quad (29)$$

which completes the closed set of dynamical equations for the system. From (25) we see that the response and the correlation functions are proportional to $\alpha^{1/4}$, thus justifying our earlier assumption that higher-order terms in the self-energies are smaller in α .

We note that (26), (27) and (29) are identical to the self-consistent equations for the $p = 4$ disordered spherical model,²⁰ which is particularly interesting since there is no *intrinsic* disorder in the periodic array described by (1) in this study. For $T > T_G$, the dynamical equations, (26), (27) and (29), can be collapsed into one equation using the fluctuation-dissipation theorem and time-translation invariance; as expected from known results on $p > 2$ spherical models,²⁰ there is a dynamical instability that is *unaccompanied* by a static transition.⁴ The introduction of higher order (in α) self-energy terms leads to dynamical equations for p disordered spherical models with several coexisting values of p (i.e. $p = 4, 6, \dots$ where $p \geq 4$ and p is even); thus this periodic array is the realization of a ‘‘simple spin glass’’ that was previously a theorist’s model system²¹ without a clear experimental counterpart. We note again that the *disordered* array previously studied⁹ is qualitatively similar to the $p = 2$ disordered XY model, and it is intriguing that the absence/presence of disorder in the array leads to the absence/presence of coinciding static and dynamical transitions.

III. THE COOLING REGIMES

The self-consistent dynamical equations, (26), (27) and (29), can be simplified substantially⁴ for temperatures $T > T_G$ where the response and the correlation functions depend *only* on the time-differences and can be related by the Fluctuation-Dissipation Theorem

$$g(t_1 - t_2) = -\frac{\partial d(t_1 - t_2)}{\partial t_1} \theta(t_1 - t_2). \quad (30)$$

Here mode-coupling theory is exact because of the absence of a length-scale in the interaction; following previous discussions of this approach²² we obtained⁴ the closed form equation

$$\int_0^\infty d(t) e^{i\omega t} \theta_t dt = \frac{1 + \int_0^\infty e^{i\omega t} d^3(t) \theta_t^4 dt}{1 - i\omega - i\omega \int_0^\infty e^{i\omega t} d^4(t) \theta_t^4 dt}. \quad (31)$$

which results in a scaling form for the relaxation time

$$t_R = t_0 \tau^{-\nu} \quad (32)$$

where $\tau \equiv \frac{\theta_G - \theta}{\theta_G}$, $\nu = 1.765$ and t_0 is a constant that can be determined numerically.⁴ This identification of the glass transition at θ_G assumes infinitesimally slow cooling from high temperatures; then the system will only fail to equilibrate when the relaxation rate diverges.

In practice the periodic array will be subject to cooling at a finite-rate. In this case, the system will fall out of equilibrium at a reduced temperature ($\theta_G^{eff} < \theta_G$) when its time-scales associated with cooling and relaxation are equivalent, namely when the condition

$$\frac{\tau}{d\tau/dt} = t_0 \tau^{-\nu} \quad (33)$$

is satisfied. (33) leads to the simple relation $\tau^{1+\nu} = t_0 \left(\frac{d\tau}{dt}\right) \approx t_0 \left(\frac{d\theta}{dt}\right)$, so that for a given finite cooling rate $\frac{d\theta}{dt}$ the array will be “out of equilibrium” for times $t > t_G^{eff}$ where

$$t_G^{eff} = t_0 \tau^{-\mu} = t_0 \left\{ t_0 \left(\frac{d\theta}{dt} \right) \right\}^{-\frac{\nu}{1+\nu}} \quad (34)$$

and undergo an effective glass transition at $\theta_G^{eff} \equiv \theta(t_G^{eff})$ which is a function of its cooling rate. In the interest of simplicity, we will no longer distinguish between the system’s effective and “adiabatic” dynamical instability; however here we wish to emphasize that their distinction is related to the finite nature of the cooling rate.

We would now like to characterize the array’s response and correlation functions at low temperatures ($\theta > \theta_G$) in its glassy regime with the hope of identifying memory and history-dependent features. Unfortunately, in the absence of time-translational invariance and the fluctuation-dissipation theorem, the solution of the self-consistent dynamical equations derived in Section II. is difficult. As already described in the Introduction, the expected behavior of $G_{tt'}$ and $D_{tt'}$ is qualitatively different for the limiting cases of fast ($t \gg t_c$) and slow cooling ($t = t_c$) regimes; here the final temperature $T_f < T_G$ is reached at time t_c . Furthermore at the onset of this study, there were no clues about the physically interesting (and experimentally accessible) crossover region where $t \gtrsim t_c$. In order to clarify this situation, we now describe our numerical studies of the dynamical equations (26), (27) and (29) in the three distinct cooling regimes. Here, in the interest of simplifying our notation, we measure all reduced temperatures in units of $\theta_G = \frac{3^{3/4}}{2^{1/2}}$ so that

$$\theta \rightarrow \theta_G \theta. \quad (35)$$

A. The Fast Cooling Regime ($t \gg t_c$)

In the limit of fast cooling all measurements are performed at times long after the system has reached its final temperature. Recently there has been progress in the characterization of infinite-range (disordered) spherical models with p -spin interactions in this regime;^{11,12} these results for the $p = 4$ case are relevant for the periodic array.

Furthermore the predicted scaling forms of the response and the correlation functions lead to physical consequences that could be experimentally observable; this will be discussed in Section IV. After a fast quench, the correlation function is predicted^{11,12} to take the form

$$d_{tt'} = f\left(\frac{t' - t_0}{t - t_0}\right) d_0 \approx \left(\frac{t' - t_0}{t - t_0}\right)^\gamma d_0 \quad (36)$$

where $t_0 = t_c + t_w$ is the time when the system reaches its final temperature ($T < T_G$; here t_c and t_w are the cooling and waiting times respectively). In Figure 3 we display $d_{tt'}$ plotted as a function of $\tilde{t} \equiv \frac{t' - t_0}{t - t_0}$ for different cooling and measurement times where $\theta_f = 1.1$ and $0 < \tilde{t} < 0.96$ corresponds to the “fast quench” regime. Short-time dynamics are observed in the range $\tilde{t} > 0.98$, and $\tilde{t} < 0$ corresponds to the “time range” when the temperature was changing at a finite rate; this range vanishes in the limit of very fast cooling. In Figure 3, we see numerical support for the scaling of the correlation function implied by expression (36); we see there that with increasing t , the correlation functions corresponding to finite-cooling rate converge to that for infinitely fast cooling. A log-log plot of the $d_{tt'}$ for the “fastest” response (with the least “tail” for $\tilde{t} < 0$) is linear, and yields $\gamma = 0.43$ and $d_0 = 0.8$ for $\theta_f = 1.1$, consistent with the numerical trends previously reported for the p -spin spherical models.^{11,12} In the case of infinitely fast cooling $t_0 = t_w + t_c$, where t_w is the waiting time at the initial (high) temperature. Furthermore we found that the correlation function for finite-rate cooling is well-described by the scaling form (36) even for relatively slow cooling rates if t_0 is adjusted so that it corresponds to the time at which the system falls out of equilibrium; now $t_0^{eff} = t_w + t_c - \delta t$.

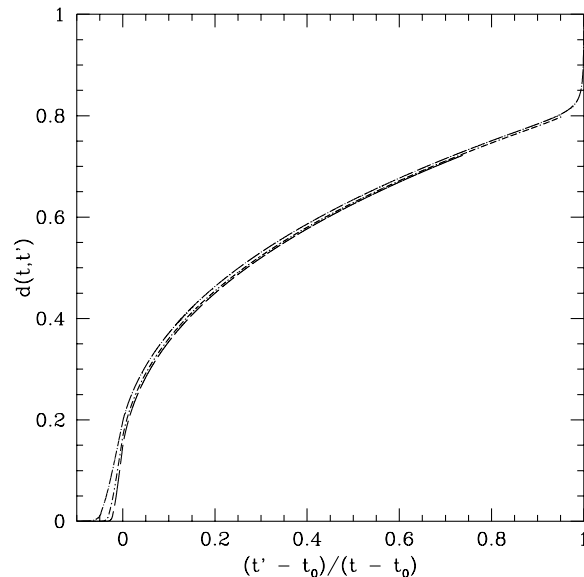


Fig 3. Numerical evidence for scaling of the correlation function $D_{tt'}$ after a fast quench to reduced temperature $\theta_f = 1.1$. The solid line corresponds to the case of an almost infinitely fast quench. The other curves correspond to a finite-cooling rate of $\frac{d\theta}{dt} = 0.05$ to the same reduced temperature with different measurement times $t=200, 300$ and 400 (top to bottom); we observe that these finite-rate correlations converge to the fast quench case with increasing t .

A generalized fluctuation-dissipation theorem (gFDT)

$$x = \frac{g_{tt'}}{d'_{tt'}} \quad (37)$$

has also been identified^{11,12} in this cooling limit for the range $0 < \tilde{t} < 1$. In Figure 4 the numerical results strongly support this proposal (note that $\tilde{t} > 0.8$ and $\tilde{t} \sim 0$ correspond to short-time dynamics and to time-interval where the temperature is varying); furthermore the value for $x = 0.55$ is in close agreement with that expected from the analytical treatment^{11,12} ($x = (p - 2)(1 - q)$ with $p = 4$ and $q = \frac{2}{3}$). We also note that the scaling form (36) appears to be robust to decreasing final temperature, though the specific values of d_0 and γ change (for $\theta_f = 1.3$, $d_0 = 0.95$ and $\gamma = 0.2$ in contrast to the values $d_0 = 0.8$ and $\gamma = 0.43$ for $\theta_f = 1.1$).

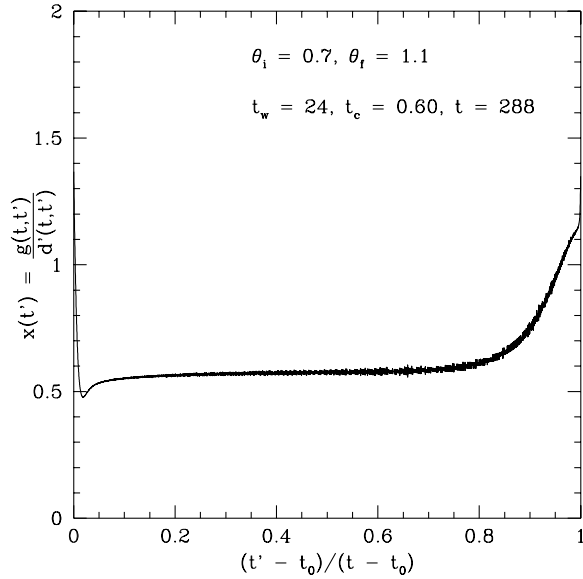


Fig 4. Numerical support for the generalized FDT relation after a fast quench. Here we plot $x(t') = \frac{g(t, t')}{d'(t, t')}$ as a function of $\tilde{t} = (t' - t_0)/(t - t_0)$ which is constant but less than unity for $\tilde{t} < 0.8$ where t_0 corresponds to the time when there is no longer temperature variation; $\tilde{t} > 0.8$ corresponds to short-time dynamics.

B. The Slow Cooling Regime ($t = t_c$)

The other limiting case is that of slow cooling where the measurement is taken at the final cooling time ($t = t_c$). We expect t^* , a time-scale that is a function of the cooling rate $\Gamma = \left(\frac{d\tau}{dt}\right)$, to play a key role in the time-dependence of the response and correlation functions; more specifically the latter will be a function of $\frac{t'}{t^*}$ and $\frac{t}{t^*}$ as displayed in Table I. where $t^* = f\left(\frac{1}{\Gamma}\right)$. The form of the functional dependence of t^* on the cooling rate must be determined numerically. In Figure 5, we plot $\frac{d_{tt'}}{\Gamma}$ and $g_{tt'}$ vs. $\Gamma t'$ where $\Gamma = \left(\frac{d\tau}{dt}\right)$ for $\theta_f = 1.1$. We remark that in the absence of anomalous scaling ($\eta = 0$), $d_{tt'}$ and $g_{tt'}$ are simply functions of the reduced temperatures θ_t and θ'_t so that in this regime they can be plotted in terms of $\tau = \theta'_t - 1$. We observe that the characteristic width decreases with increasing cooling times suggesting the need for another functional form for Γ . In Figure 6, we present another scaling plot for the same data as in Figure 5 ($\theta_f = 1.1$); this time we plot $\frac{d_{tt'}}{\Gamma}$ and $g_{tt'}$ vs. $\tilde{\Gamma} t'$ where $\tilde{\Gamma} = \Gamma^{1-\eta}$ with $\eta = 0.19$; now the curves fall on top of one another nicely. In this case $d_{tt'}$ and $g_{tt'}$ are *not* just functions of the reduced temperatures. Scaling plots are also presented for data associated with $\theta_f = 1.2$ and $\theta_f = 1.3$ in Figures 7 and 8; we infer from these results that

$$t^* = \left(\frac{1}{\Gamma}\right)^{1-\eta(T)} \quad (38)$$

where η decreases with decreasing temperature. More specifically we find that $\eta = 0.19, 0.12$ and 0.0 for $\theta_f = 1.1, 1.2$ and 1.3 , and the associated scaling plots are displayed in Figures 6 - 8. In Figures 6 and 7 $\eta \neq 0$ and there is a new time-scale, t^* , associated with the decay of the correlation functions. The scaling plots in Figure 8 indicate that $\eta = 0$ at lower temperatures, suggesting that the array “rejuvenates” and improves its memory there. We note that $\eta = 0$ in the slow cooling regime of the Sherrington-Kirkpatrick model;¹³ it is somewhat amusing that such ageing effects,^{23,24} well-known in spin glasses, should appear in a model for a periodic array. The observable consequences of this “forgetfulness” and subsequent “rejuvenation” will be discussed in Section III. Finally we note that at temperatures such that $\eta = 0$ $\frac{\partial d(t, t')}{\partial t'}$ is constant for a wide temperature range resembling the slow cooling solution of the Sherrington-Kirkpatrick model¹³. We also recall that there were no qualitative changes in the fast-cooling regime as a function of increasing θ_f (decreasing temperature).

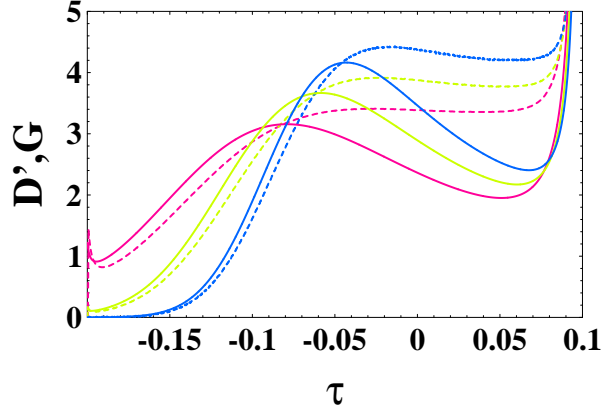


Fig 5. Absence of the adiabatic limit in the slow cooling regime. Here we plot $\frac{1}{\Gamma} \frac{\partial d(t, t')}{\partial t'}$ and $\frac{1}{\Gamma} g(t, t')$ vs. $\tau = \Gamma(t' - t_G) = \theta(t') - 1$ for different cooling rates ($\Gamma = 0.3/40, 0.3/80$ and $0.3/160$); the characteristic width of the curves decreases with increasing cooling times. All dashed curves are $d'(t, t')$ and the solid ones are $g(t, t')$, and the cooling time increases from bottom to top.

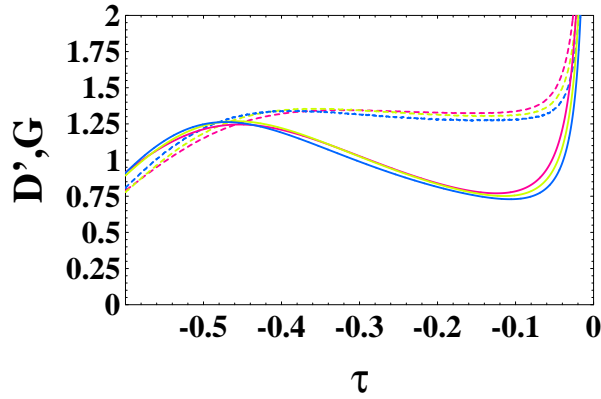


Fig 6. A scaling plot of $\frac{1}{\tilde{\Gamma}} \frac{\partial d(t, t')}{\partial t'}$ vs $\tau(t') = \tilde{\Gamma}(t' - t)$ for three different cooling rates ($\Gamma = 0.3/40, 0.3/80$ and $0.3/160$) where $\tilde{\Gamma} = \Gamma^{1-\eta}$ with $\eta = 0.19$; here $\theta_f = 1.1$ All dashed curves are $d'(t, t')$ and the solid ones are $g(t, t')$.

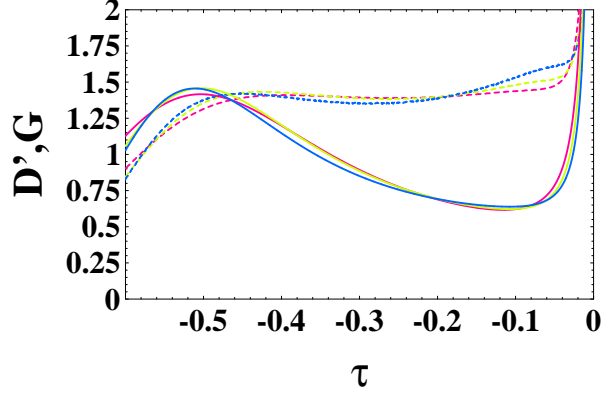


Fig 7. A scaling plot of $\frac{1}{\tilde{\Gamma}} \frac{\partial d(t, t')}{\partial t'}$ vs $\tau(t') = \tilde{\Gamma}(t' - t)$ for three different cooling rates ($\Gamma = 0.3/40, 0.3/80$ and $0.3/160$) where $\tilde{\Gamma} = \Gamma^{1-\eta}$ with $\eta = 0.12$; here $\theta_f = 1.2$. All dashed curves are $d'(t, t')$ and the solid ones are $g(t, t')$.

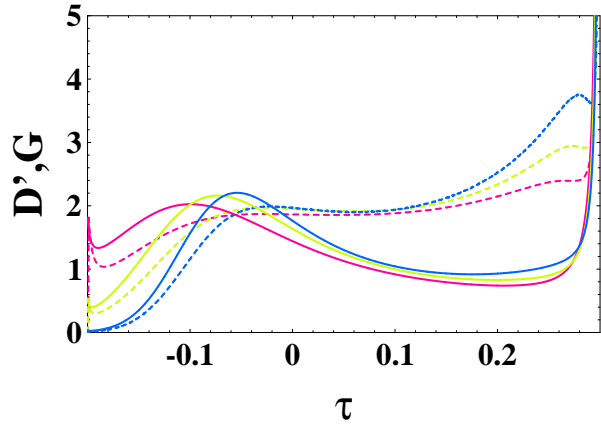


Fig 8. A scaling plot of $\frac{1}{\Gamma} \frac{\partial d(t, t')}{\partial t'}$ vs $\tau(t') = \Gamma(t' - t_G) = \theta(t') - 1$ for three different cooling rates ($\Gamma = 0.3/40, 0.3/80$ and $0.3/160$) indicating the appearance of the adiabatic limit at $\theta_f = 1.3$. All dashed curves are $d'(t, t')$ and the solid ones are $g(t, t')$, and the cooling time increases from bottom to top.

C. The Crossover Cooling Regime ($t > t_c$)

As indicated in Table I, we had no initial expectations for the form of $d_{tt'}$ and $g_{tt'}$ in the intermediate cooling regime $t \gtrsim t_c$. In Figure 9 we display a number of correlation functions that display crossover behavior between the two limits of the fast and slow cooling cases. Here we see that at $t \gtrsim t_c$ there exist at least two distinct regimes: $t' < t_0$ and $t' > t_0$. In the first regime $\frac{\partial d}{\partial t'}$ is approximately constant, whereas in the second case the correlation function varies more like a power-law resembling the fast cooling case. In order to emphasize this point, we have included a scaling curve $D(t') = d_0 \left(\frac{\tilde{t}-x}{1-x} \right)^\gamma$ where $\tilde{t} = \frac{t'-t_0}{t-t_0}$; here $x = 0.13$ is parameter that effectively rescales t_0 , and we have taken the parameters $d_0 = 0.8$ and $\gamma = 0.43$ from the fast-cooling case (see Figure 3) where $\theta_f = 1.1$. We note that the scaling curve and the correlation function ($t = 432$) agree very well for $\tilde{t} > 0.3$; we also see an intermediate regime $0 < \tilde{t} < 0.3$ where there is still curvature in $D(t')$ but no agreement with the scaling form (36). The generalized FDT ratio x , displayed in Figure 10, is as previously observed for fast cooling (cf. Figure 4) for $\tilde{t} = \frac{t'-t_0}{t-t_0} > 0$, but is no longer constant for $\tilde{t} < 0$ (slow cooling). By contrast in Figure 11 we observe that $\frac{\partial d(t,t')}{\partial t'}$ is almost constant as in the slow-cooling regime discussed above (see Figs 5-7). This overall behavior suggests that for “crossover measurement times” ($t \gtrsim t_c$), the system’s behavior is a combination of that observed for both fast and slow cooling. As discussed in Section IIB, the behavior of the slow-cooling correlation function changes qualitatively when the final temperature is sufficiently low ($\theta_f \geq 1.3$). This change also affects the correlation function in the crossover regime. As we observe in Figure 12 the $\frac{\partial d(t,t')}{\Gamma \partial t'}$ acquires a peak and, more importantly, it ceases to depend on the cooling rate Γ indicating that the system preserves its memory of the cooling process even as $t \rightarrow \infty$ (with the ratio $\frac{t}{t_c}$ maintained constant). We note that the plateau displayed in Figure 12 corresponds to that of d' shown in Figures 7 and 8 (in the slow cooling regime). The range $\tilde{t} = \frac{t'-t_0}{t-t_0} > 0$ corresponds to the fast cooling regime where $\frac{\partial d}{\partial t'} \sim \frac{1}{t'}^{\gamma-1}$; the observed peak is needed to match the fast- and slow- cooling regimes.

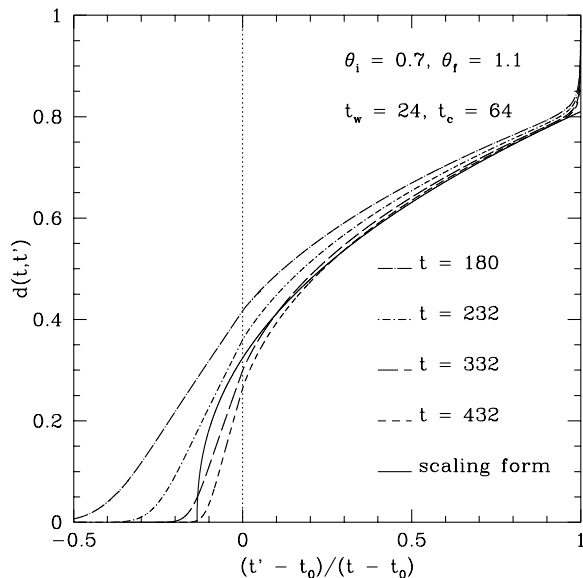


Fig 9. The correlation function $d(t, t')$ in the crossover between fast and slow cooling regime for cooling rate $\Gamma = 0.0125$ and $t = 180, 232, 332, 432$ and $\theta_f = 1.1$ (top to bottom). Note the presence of two different regimes evident for $t \sim t_c$: (1) $\frac{\partial d(t,t')}{\partial t'} \approx$ constant for $\tilde{t} < 0$ and (2) power-law variations at $\tilde{t} > 0$ resembling the fast cooling regime where $\tilde{t} = \frac{t'-t_0}{t-t_0}$. Note that at t becomes larger than t_c the linear slow-cooling regime rapidly vanishes and that the correlation function converges to the scaling form (36) (dash-dot curve) $D = d_0 \left(\frac{\tilde{t}-x}{1-x} \right)^\gamma$ with $d_0 = 0.8$, $\gamma = 0.43$ and $x = -0.13$.

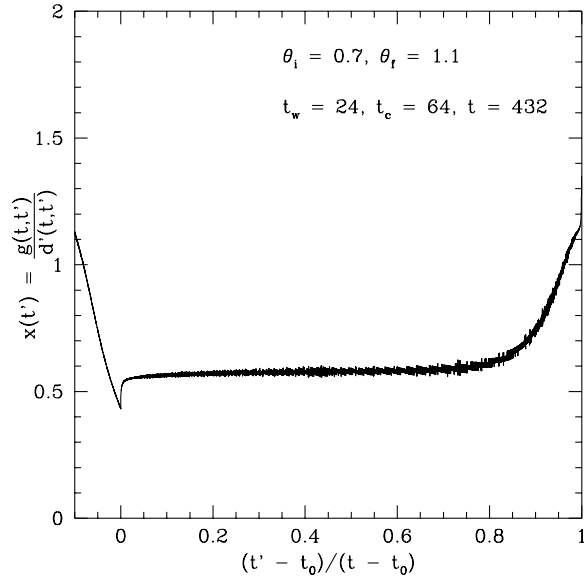


Fig 10. The generalized FDT ratio x in the crossover regime between slow and fast cooling for $\Gamma = 0.125$, $t = 432$ and $\theta_f = 1.1$. Note that in this plot t was sufficiently larger than t_c and the modified FDT relation is maintained for most of the range $((t' - t_0)/(t - t_0) > 0)$; furthermore x is as previously observed for fast cooling, but for $(t' - t_0)/(t - t_0) < 0$ the ratio is no longer constant.

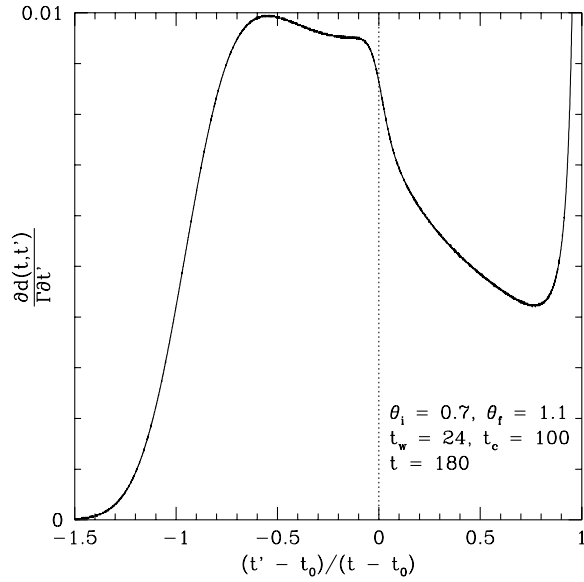


Fig 11. The derivative of the correlation function, $\frac{\partial d(t, t')}{\Gamma \partial t'}$ for $\Gamma = 0.004$, $t = 180$ and $\theta_f = 1.1$ in the crossover between slow and fast cooling. In this figure $t \sim t_c$ and we see the appearance of the behavior characteristic of slow cooling ($\frac{\partial d(t, t')}{\partial t'} \approx \text{constant}$).

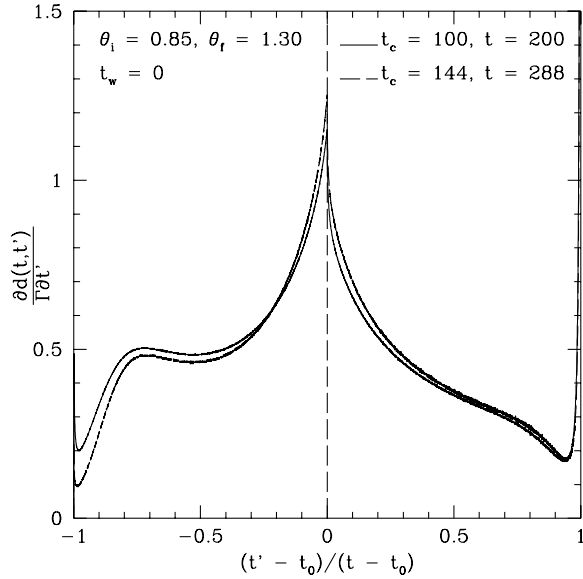


Fig 12. The derivative of the correlation function, $\frac{\partial d(t, t')}{\Gamma \partial t'}$ for two cooling rates, $\Gamma = 0.45/100, .45/144$ with the same ratio $\frac{t}{t_0} = 2$ and $\theta_f = 1.3$. We see that $\frac{\partial d(t, t')}{\Gamma \partial t'}$ is constant even in the slow cooling regime indicating “perfect” memory.

D. Non-Monotonic Cooling and Structure of the Phase Space

It is known that the structure of the metastable states in the (disordered) Sherrington-Kirkpatrick (SK) model is rather complex; the states are arranged on an ultrametric tree with many branch points. Here we provide evidence that the situation is rather different for the periodic array discussed here. In the glassy phase of the SK model, each metastable state subdivides and “daughter” states appear as the temperature is lowered. In this case application of a heat pulse removes some of this subdivision and results in a partial loss of memory. For the periodic array such behavior is *not* observed but, by contrast, a small heat pulse does not lead to any aftereffect. Of course a large heat pulse brings the system to above its effective glass transition temperature and thus erases *all* of its memory. In Figure 13 we display the correlation functions for varying amplitudes of applied heat pulses. Here the system was cooled fast to low temperature ($\theta = 1.4$), equilibrated and then subjected to a heat pulse. From the results shown in Figure 13 we conclude that a small heat pulses does not change the state of the array at $\theta \ll \theta_G$, while a large one brings it above the effective glass transition temperature and eliminates all memory of its initial state. If the metastable states did subdivide with decreasing temperature, the correlation and response functions obtained with and without the application of a moderate heat pulse would be different; in the former case memory of some of the subdivisions would be erased. Clearly this is not the case for the periodic array, and response functions for this cooling-heating process (not shown) are also consistent with this conclusion. Furthermore, we checked that the results obtained when the system was cooled slowly to $\theta = 1.4$, equilibrated and then subjected to the heat pulse were qualitatively similar. From these results we conclude that there is *no* subdivision of metastable states below the glass transition temperature.

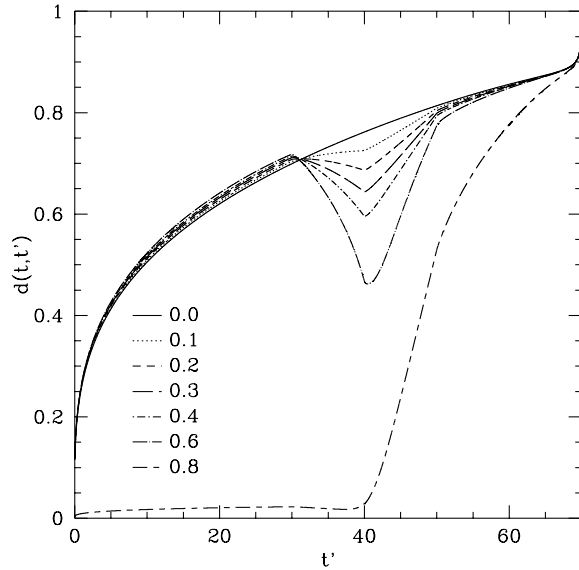


Fig 13. The correlation function, $d(t, t')$, for the cooling-heating regime. Here the temperature was reduced infinitely fast to $\theta = 1.4$ at $t' = 0$; the system was equilibrated for $0 < t' < 30$, then heated linearly for $30 < t' < 40$, then cooled linearly back to $\theta = 1.4$ for $40 < t' < 50$ and then measured at $t = 70$. Different curves correspond to different amplitudes of the heat pulse as shown. We see that for heat pulses of amplitude less than 0.6 the system recovers its original state; however for larger heat pulses all memory is lost.

We also checked that these results were not due to the leading-order approximations made in the derivation of the dynamical equations, and thus performed direct simulations of the array to confirm that this conclusion remains valid at low temperatures and at large α . First we simulated finite-size arrays with $\alpha = 1.0$ at very low temperatures and confirmed that the number of metastable states grows exponentially with system-size. We also studied the distribution of overlaps between these states, and our results are displayed in Figure 14 for $\alpha = 1.0$. Here we see that the overlap distribution evolves to a sharp peak with a maximum that shifts to lower q with increasing number of wires N . In particular we do not observe any states with large overlaps for $N \geq 15$; furthermore $P(q)$ suggests that for large values of N the states are equidistant in phase space. We also found qualitatively similar results for smaller values of α .

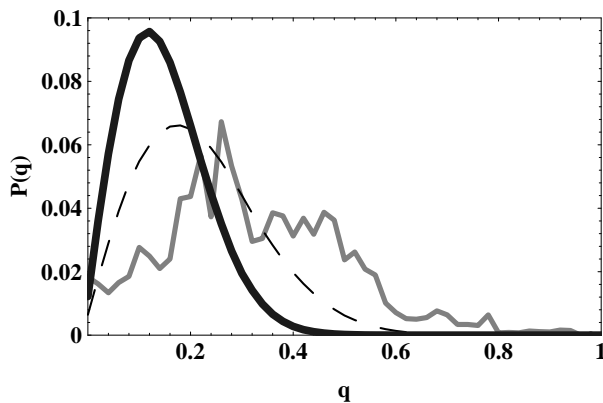


Fig 14. Distribution of overlaps for finite-size arrays with $\alpha = 1.0$. Here the gray, dashed and black curves correspond to $N = 7, 15$ and 31 respectively.

The equidistance of metastable states does not imply that the structure of the phase space is simple. In particular the basins of attraction associated with different metastable states appear to be complicated. For example, we have studied the probability, $Q(q)$, that a randomly chosen state that has overlap q with a metastable one evolves to this particular metastable state. The results are displayed in Figure 15. We see that the probability to evolve to *different* states remains finite even if the starting overlap is close to unity. Our results suggest that $1 - Q(q) \propto (1 - q)$ for $N \rightarrow \infty$. If true, this has important consequences for the distribution of barriers. First we note that the energy required to flip m spins cannot be larger than mT_0 . The probability of evolving to a different metastable state after the flipping of m spins is roughly $\frac{m}{N}$ so the probability to find *some* m spins which lead to this result is $O(1)$. This implies that even in the infinite-range periodic system there is a broad distribution of barriers which extend down to $E_B \sim T_0$. We note that this result implies that the distribution of barriers and overlaps are *not* related.

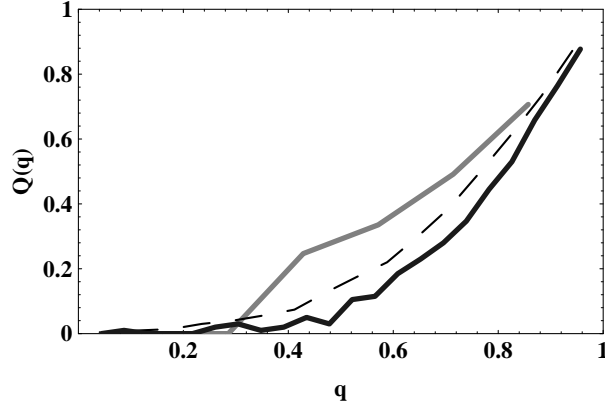


Fig 15. The probability, $Q(q)$, to evolve back to a metastate state, A , starting with a randomly chosen state with overlap q with state A . The data shown here are the results of a direct numerical simulations of a finite size arrays with $\alpha = 1.0$; the gray, dashed and black curves correspond to $N = 7, 17$ and 23 respectively.

IV. THE PHYSICAL CONSEQUENCES

What are the observable consequences of the different behavior in the response and the correlation functions for the three cooling regimes? If the periodic array is placed in a time-dependent field $H(t)$ that is small compared to its constant part, the resulting Josephson currents generate a total magnetic moment

$$M_t = \mu \int_{-\infty}^t g_{tt'} d_{tt'} \{H(t) - H(t')\} dt' \quad (39)$$

which can be measured with an inductance coil; here

$$\mu = \left(\frac{2e}{\hbar e}\right)^2 \left(\frac{L^2}{12}\right)^2 N \left(\frac{J_0^2}{T}\right) \frac{1}{\alpha^2} \left(1 - \frac{J_0^2}{A^2 \alpha}\right) \left(\frac{t_0}{\alpha^{1/2} \theta_t}\right) \quad (40)$$

where $L = Nl$. The form of M in (39) should be contrasted with the response of the spin system to a physical magnetic field which is just $g_{tt'}$; the dissimilarity is due to the fact that in the Josephson array *direct* coupling of the physical field to the “spins”, $s_i = e^{i\phi}$, is prohibited by gauge invariance. Instead H couples to the network via changes of the Josephson exchanges; hence the response involves a four-spin term (GD). Here we discuss the magnetization induced by a small increment of magnetic field applied at time t_H ; this is of course the simplest possible case. Still the value of the observed moment will depend on the relative magnitudes of t_H , t_c , t^* and t as indicated in the schematic of Figure 16. We proceed to discuss each separate case below.

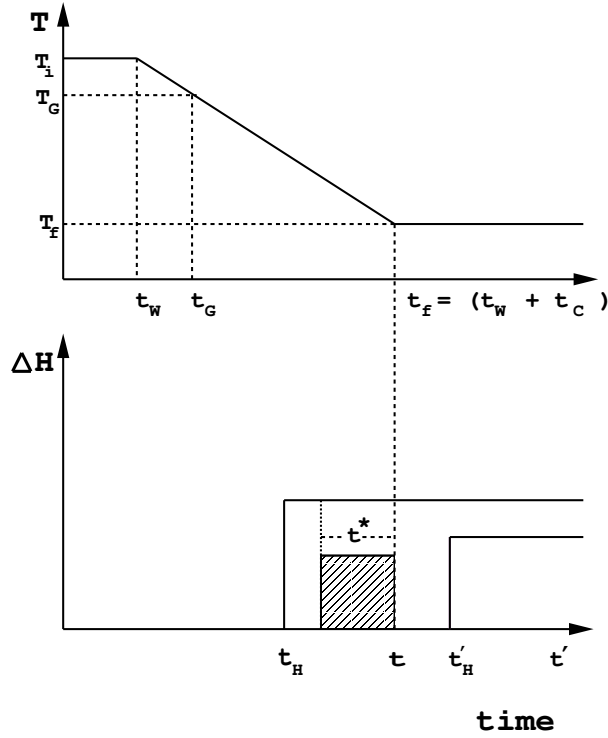


Fig 16. Schematics of (a) Temperature (T) (b) Application of an Additional Field (ΔH) vs time indicating the time-scales involved in a finite-cooling experiment as discussed in the text; T_G and t_G refer to the temperature and time when the system goes out of equilibrium, and t_H and t^* are the time-scales associated with the onset of an additional field and ageing; t is the total time associated with a given measurement.

A. $t, t_H \gg t_c$

Here we apply a field after a fast quench, a regime where there is a generalized fluctuation dissipation relation. Then the expression for the moment in (39) becomes

$$M = \mu x \int_{t_c \sim 0}^{t_H} \frac{1}{2} (D^2)' \Delta H dt' = \frac{\mu}{2} x d_0^2 \left(\frac{t_H - t_G}{t - t_G} \right)^{2\gamma} \Theta(t_H - t_G) \Delta H \quad (41)$$

where we have used the “fast cooling” scaling form for the correlation function exhibited in Table I. Since the fast-cooling response function decays with time, (41) indicates an “ageing” moment which decreases as a function of decreasing ratio $\frac{t_H - t_G}{t - t_G}$ ($t_H, t > t_G$). (41) also implies markedly different behavior if $t_H > t_G$ or $t_H < t_G$; this is the array analogue of the standard zero-field vs. field cooled susceptibility measurement often performed on spin glasses.²⁴

B. $t_H < t_c = t$

Now the cooling is continued after the field application (cf. Figure 13), and the dominant contribution to the expression for the moment, (39), will come from the range $t_c - t^* < t' < t_c$ where t^* is the “ageing” time-scale discussed in the slow cooling regime in Section III. Here there are two possibilities:

(a) $t_c - t_H < t^*$

In this case the correlation and the response functions are non-decaying (cf. Figs. 4-7) and the moment is a constant as in (42).

(b) $t_c - t_H > t^*$

The correlation and response functions have no memory on time-scales greater than t^* ; therefore the moment is zero. The system is displaying ageing analogous to that observed in spin glasses;²⁴ as in the latter case, there appears to be a “rejuvenation” associated with improved memory at low temperatures where t^* increases.

We also remark that application of a a.c. field could lead to a direct experimental determination of $G_\omega D_\omega$; there we expect $\chi''(\omega) \sim f(\omega t^*)$ as shown below in Figure 17. Here we define $\chi(\omega) = \int_{-\infty}^t dt' \exp^{i\omega(t-t')} d_{tt'} g_{tt'}$.

We note that the low-frequency part of the displayed curves is universal and so would provide an experimental determination of the time-scale associated with ageing, t^* .

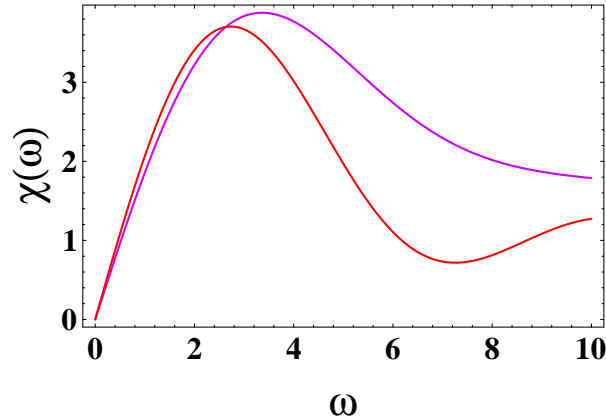


Fig 17. Typical imaginary parts of ac susceptibility for the slow cooling processes. Here we show the results for the cooling rates $\Gamma = 0.00057$ (upper curve) and $\Gamma = 0.0022$ (lower curve). The upper curve shows imaginary part of susceptibility measured at reduced temperature $\theta_f = 1.0$; the lower curve corresponds to the measurement at $\theta_f = 1.2$. The frequency ω is measured in units of the inverse characteristic time, $t^* = 120$, corresponding to the decay of the correlation function. Here we define it by the following procedure: (i) we do a linear fit to $d_{tt'}$; (ii) we identify the intersection of this approximated version of $d_{tt'}$ and the x-axis as $t - t^*$. Using this definition, t^* acquired the identical value for the two cooling processes considered here.

C. $t > t_c > t_H$

In this “crossover regime” the incremental time-dependent field is applied before the system has reached its final cooling temperature ($T_f < T_G$); then the expression for the moment becomes

$$M \sim \int_{t_G}^{t_H} \tilde{\Gamma} G[\tilde{\Gamma}(t-t')] D[\tilde{\Gamma}(t-t')] \Delta H dt' = \mu_A \Delta H \quad (42)$$

where μ_A is a number; this result is obtained by changing the integration variable to $\tilde{t} = \tilde{\Gamma} t'$ where $\tilde{\Gamma} \sim \left(\frac{dT}{dt}\right)^{1-\eta(T_f)}$. In this regime the moment is simply a constant with no time-dependence but with possible dependence on the cooling rate if $\eta \neq 0$.

V. CONCLUDING DISCUSSION

In conclusion we have studied history-dependence and ageing in a periodic model in the *absence* of disorder. In the case of a fast quench ($t \gg t_c$) a generalized fluctuation dissipation theorem relation ($G \sim xD'$) exists between the correlation and the response functions, and furthermore the latter exhibit a predicted scaling form.¹¹ In the other limit of slow cooling ($t = t_c$) there is numerical evidence for the existence of an “ageing” time-scale t^* such that for $t > t^*$ the system forgets its past, but for $t < t^*$ it has “perfect memory”. This additional time-scale increases to that associated with the cooling process with decreasing temperature, indicating that at low temperatures the system recovers its memory and an adiabatic solution (cf. Table I) reappears. However the form of this solution does not resemble (cf. Fig. 8) the “adiabatic ansatz”¹⁵ $G \sim \delta$ and $D \sim D_0$, which is probably *never* correct. We speculate that this is due to the presence of an extensive number of states exactly at the glass transition, where the time-scale associated with the cooling process is significantly less than that of the system’s relaxation. By contrast, in the Sherrington-Kirkpatrick model such “branching of states” occurs at lower temperatures where the cooling and relaxation times are comparable; in this case the assumption that there are no additional time-scales¹³ leads to results which agree with those obtained by thermodynamic methods.²⁵

We also speculate on two different scenarios for the decrease of the exponent η ($t^* = \left(\frac{dt}{d\tau}\right)^{1-\eta(T)}$) with decreasing temperatures, and the reappearance of the adiabatic solution. One is that the latter solution is always present for $\theta > \theta_G$, but its weight is proportional to a high power of $\theta - \theta_G$, and thus is only observable at lower temperatures. Another possibility is that $\eta \rightarrow 0$ corresponds to a second dynamical transition at lower temperatures. Below the temperature associated with this second dynamical instability the metastable states would not evolve dramatically with subsequent cooling, leading to the absence of further ageing effects. Naturally the emergence of t^* from an analytic ansatz for the dynamical equations would provide additional insight to this issue. Unfortunately these equations are difficult to solve in the slow-cooling regime since the corrections to long-time behavior are of the same order as the leading terms themselves.

Just below its glass transition temperature, the periodic array becomes stuck in one of an extensive number of metastable states that are equidistant in phase space. Our numerical studies indicate that there is *no further subdivision* of these states at lower temperatures, in contrast to the situation for the (disordered) Sherrington-Kirkpatrick model. However the probability to evolve to different metastable states remains finite even if the starting overlap is very close to unity, which suggests that the distribution of barriers and the overlaps are *not* simply related. It would be interesting to know if these features of the periodic array’s low-temperature phase space are signatory of a glass with distinct dynamic and static transitions.

Naturally there remain several questions to be addressed in future projects. A key feature of this periodic array is that it can be realized experimentally;⁸ a calculation and subsequent experimental determination of its nonlinear response be quite interesting. In a real system there are everpresent induced screening currents ignored in the present treatment, and the addition of these terms could lead to novel memory effects. Amusingly enough, ageing effects are not present in the disordered long-range array; a study of the crossover between the periodic and the random networks might provide further insight into the origin of this widespread but mysterious phenomenon.

We would like to acknowledge useful discussions with J. Kurchan, D. Sherrington, M. Stephens, and thank A. Schweitzer for his help in optimizing the numerical code. Financial support via the grants from RFBR # 95-02-05720 and INTAS-RFBR # 95-0302 (M.V.F. and D.M.K.) and via DGA grant # 94-1189 (M.V.F.) is gratefully acknowledged. M.V. Feigelman and D.M. Kagan thank NEC for hospitality.

¹ e.g. T.R. Kirkpatrick and D. Thirumalai, PRB **36**, 5388 (1987); J.P. Bouchaud and M. Mezard, J. Phys. I **4**, 1109 (1994); S. Franz and J. Herz, PRL **74**, 2115 (1995); L.F. Cugliandolo, J. Kurchan, R. Monasson and G. Parisi, J. Phys. A **29**, 1347 (1996).

² e.g. E. Marinari, G. Parisi and F. Ritort, J. Phys. A, **28**, 4481 (1995); M. Potters and G. Parisi, J. Phys. A **28**, 5267 (1996) and references therein.

³ P. Chandra, L. B. Ioffe and D. Sherrington, Phys. Rev. Lett. **75**, 713 (1995).

⁴ P.Chandra, M.V. Feigelman and L.B. Ioffe, Phys. Rev. Lett. **76**, 4805 (1996).

⁵ D.J. Thouless, P.W. Anderson and R.G. Palmer, Phil. Mag., **35**, 593 (1977).

⁶ M. Stephens and D. Lidsky, unpublished.

⁷ M.R. Schroeder, *Number Theory in Science and Communication*, (Springer-Verlag, 1986).

- ⁸ P. Chandra, M.V. Feigelman, M.E. Gershenson and L.B. Ioffe, to be published in *Proc. Sitges XIV Conference*, ed. M. Rubi, (Springer-Verlag, 1996).
- ⁹ V. M. Vinokur, L. B. Ioffe, A. I. Larkin, M. V. Feigelman, *Sov. Phys. JETP* **66**, 198 (1987).
- ¹⁰ D. Sherrington and S. Kirkpatrick, *Phys. Rev. B* **35**, 1792 (1975).
- ¹¹ L.F. Cugliandolo and J. Kurchan, *Phys. Rev. Lett.* **71**, 173 (1993).
- ¹² L.F. Cugliandolo and J. Kurchan, *J. Phys. A.: Math. Gen* **27**, 5749 (1994).
- ¹³ L. Ioffe, *Phys. Rev. B* **38**, 5181 (1988).
- ¹⁴ H.-J. Sommers, *J. Phys. (Paris) Lett.* **46**, L779 (1985).
- ¹⁵ M.V. Feigelman and D.M. Kagan, *Sov. Phys. JETP* **82**, 1129 (1996) (*ZhETF*, **109**, 2094 (1996)).
- ¹⁶ C. De Dominicis, *J. Phys. (Paris) C*, **1**, 247 (1976); C. De Dominicis and L. Peliti, *Phys. Rev. B*, **18**, 353 (1978).
- ¹⁷ H.K. Janssen, *Z. Phys. B* **23**, 377 (1976); R. Bausch, H.K. Janssen and H. Wagner, *ibid* **24**, 113 (1976).
- ¹⁸ H. Sompolinsky and A. Zippelius, *Phys. Rev. B*, **25**, 6860 (1982).
- ¹⁹ P.C. Martin, E.D. Siggia and H.A. Rose, *Phys. Rev. A* **18**, 353 (1978)
- ²⁰ A. Crisanti, H. Horner, H.-J. Sommers, *Z. Phys. B*, **92**, 257 (1993).
- ²¹ D. Gross and M. Mezard, *Nucl. Phys. B*, **297**, 74 (1985).
- ²² W. Gotze, *Z. Phys. B* **56**, 139 (1984); E. Leutheusser, *Phys. Rev. A* **29**, 2765 (1984).
- ²³ E. Vincent, J. Hamman, M. Ocio, J.-P. Bouchaud and L. F. Cugliandolo, to be published (cond-mat/9607224).
- ²⁴ K.H. Fischer and J.A. Hertz, *Spin Glasses*, (Cambridge University Press, 1991).
- ²⁵ M. Mezard, G. Parisi and M.A. Virasoro, *Spin Glass Theory and Beyond*, (World Scientific, Singapore 1987).